European Journal of Pharmacology 1002 (2025) 177864

Contents lists available at ScienceDirect

European Journal of Pharmacology

journal homepage: www.elsevier.com/locate/ejphar

Comparative analysis of the antiglioblastoma activity of adenosine A_{2A} receptor and CK1δ blockers

Akshaya Murugesan [a,b], Anxo Vila Alonso [a,b], Saravanan Konda Mani [c], Puja Sarkar [a], Aleksei Smirnov [d], Beatrice Francucci [d], Gabriella Marucci [d], Michela Buccioni [d], Kasim S. Abass [e], Chandrabose Sureka [f], Olli Yli-Harja [g], Meenakshisundaram Kandhavelu [a,b,*]

[a] Molecular Signaling Group, Faculty of Medicine and Health Technology, Tampere University, Tampere, 33710, Finland
[b] BioMeditech and Tays Cancer Center, Tampere University, Hospital, P.O. Box 553, 33101, Tampere, Finland
[c] B-Aatral Biosciences Private Limited, Bangalore, 560091, Karnataka, India
[d] Medicinal Chemistry Unit, School of Pharmacy, University of Camerino, 62032, Camerino, Italy
[e] Department of Physiology, Biochemistry and Pharmacology, College of Veterinary Medicine, University of Kirkuk, 36003, Iraq
[f] Department of Basic Medical Sciences, College of Medicine, Prince Sattam Bin Abdulaziz University, Al-Kharj, 11942, Saudi Arabia
[g] Computaional Systems Biology Group, Faculty of Medicine and Health Technology, Tampere University, Tampere, 33710, Finland

ARTICLE INFO

Keywords:
Adenosine A2A receptor
Casein kinase 1δ kinase domain
In silico
Cell death
3D spheroids

ABSTRACT

Glioblastoma multiforme (GBM), a multifactorial deadliest cancer with constrained clinical efficacy due to heterogeneity, drug resistance, side effects of the chemotherapeutic drug, necessitating the development of novel cancer therapeutics. The adenosine A_{2A} receptor targeted binding of antagonist leads to regulation of downstream effectors, mediating the phosphorylation of Casein kinase 1δ kinase domain (CK1δ) in cancers. Here, we performed a comparative investigation of Food and Drug Administration (FDA) approved drugs, istradefylline and riluzole inhibiting adenosine A_{2A} receptor and CK1δ isoform in GBM cell growth. Molecular interaction of riluzole with CK1δ isoform and istradefylline with adenosine A_{2A} receptor was identified through molecular docking and dynamic simulations. The potential of these two FDA approved drugs in inhibiting GBM cell growth was investigated through various in-vitro analysis including dose-dependent dynamic assay, cell cycle assay, apoptosis assay by flow cytometry. Further the effect of these drugs on spheroid cell growth and cell size was measured. *In silico* analyses demonstrated that riluzole binds strongly to CK1δ isoform with a binding energy of −9.02 kcal/mol, whereas istradefylline binds to adenosine A_{2A} receptor with −9.88 kcal/mol. *In vitro* evaluation revealed that riluzole increased cell growth inhibition by 24 % in LN229 cells and 36 % in SNB19 cells than istradefylline. Riluzole arrested the cell cycle at S phase in both cell lines, whereas istradefylline arrest was cell line specific. Three-dimensional (3D) spheroid model of 1321N1 GBM cells further demonstrated that riluzole inhibits ~50 % higher cell growth inhibition than istradefylline with effective reduction in spheroid volume and size. Overall, our analysis revealed that blocking of adenosine A_{2A} receptor downstream signaling pathway protein CK1δ with its inhibitor, riluzole, showed higher anti-GBM effect than its upstream signaling blocker, istradefylline. Thus, blocking adenosine A_{2A} receptor downstream effector signaling protein through its antagonist and blocking its effector protein CK1δ could provide an opportunity to develop targeted therapy for GBM.

1. Introduction

Glioblastoma (GBM), the lethal malignant brain tumor worldwide has an overall survival rate of 6.8 % (Ostrom et al., 2019). The treatment strategy currently includes surgical resection along with radiation therapy, chemotherapy, and adjunctive use of tumor-treating field (TTF) technology (Kast et al., 2013; Cantrell et al., 2019). Despite of the multimodal approach such as advancements in surgical imaging techniques (Wu et al., 2021) for extensive removal of tumor tissue, the use of Optune®, a medical device that creates low-intensity and alternating

* Corresponding author. Molecular Signaling Group, Faculty of Medicine and Health Technology, Tampere University, Tampere, 33710, Finland.
E-mail address: meenakshisundaram.kandhavelu@tuni.fi (M. Kandhavelu).

https://doi.org/10.1016/j.ejphar.2025.177864
Received 17 March 2025; Received in revised form 19 June 2025; Accepted 19 June 2025
Available online 20 June 2025

tumor treating fields, stereotactic radiosurgery and brachytherapy (Mehta et al., 2017) to control brain metastases, the overall survival rate and quality of life remains poor. Several drugs approved by the Food and Drug Administration (FDA) for GBM treatment at various stages of clinical trials, together with their targets and associated effects, are detailed in Table 1. Traditional drug development for GBM is hindered due to its high cost and low success rate; hence, repurposing drug is considered as a significant alternative and a novel approach (Hernandez et al., 2017).

Adenosine receptors (AR), A_1, A_{2A}, A_{2B}, and A_3, play an important role in neuroinflammatory disorders and the development and progression of various cancers, including glioblastoma. Among the four AR's, adenosine A_{2A} receptor inactivation protects the brain by inhibiting glutamate release and suppressing proinflammatory cytokines (Popoli et al., 2002). adenosine A_{2A} receptor signaling activation leads to the activation of the phosphatidylinositol 3-kinase (PI3K)/protein kinase B (AKT) signaling pathway (Ma et al., 2019), with the involvement of phosphorylated AKT (pAKT) in tumor cell transition, anti-apoptosis and promotion of tumor cell growth and metastasis (Chen et al., 2007; Sasaki and Kuniyasu, 2014; Jacobson et al., 2021). Blockade of the adenosine A_{2A} receptor signaling pathway with potential antagonist inhibits protein kinase C isoform α (PKCα), that mediates phosphorylation of a downstream signaling protein, Casein kinase 1δ kinase domain (CK1δ). Notably, CK1δ alone is considered as a promising target for several pathophysiological processes including neurodegenerative diseases, cancer, cytokinesis, cell cycle progression, apoptosis, DNA damage response, and RNA metabolism. Besides autophosphorylation, CK1δ is also phosphorylated by other kinases including PKA (cAMP--dependent protein kinase), Akt (protein kinase B), CLK2 (CDC-like kinase 2), PKCα, and Chk1 (checkpoint kinase 1).

However, the comparative effectiveness of adenosine A_{2A} receptor and CK1δ inhibition in glioblastoma, thereby inducing GBM cell death is not yet reported. Thus, the present study is focused on exploring the effect of currently available FDA-approved drugs, riluzole and istradefylline, which could either effectively inhibit CK1δ isoform and/or adenosine A_{2A} receptor respectively, which would improve the treatment modality against GBM. Riluzole belong to the 2-aminobenzothiazole family of widespread oral drug for the fatal neurodegenerative disorder amyotrophic lateral sclerosis (ALS)(Saitoh and Takahashi, 2020), and is reported to be a ATP-competitive inhibitor for the protein kinase CK1 isoform δ (Bissaro et al., 2018).

Numerous studies have explored the mechanism by which riluzole could also target a number of cancer types including pancreatic cancer (Sun et al., 2021), colorectal cancer(Fortunato, 2017), melanoma (Namkoong et al., 2007), prostate cancer(Wadosky et al., 2019), breast cancer(Speyer et al., 2017), glioblastoma(Benavides-Serrato et al., 2020a), and lung cancer(Lemieszek et al., 2018). Riluzole inhibits GBM cell growth by reducing glucose transporter 3 (GLUT3) transporter expression, thereby modulating the metabolic activity of the cell by altering the phosphorylation of AKT (Sperling et al., 2017). Another noteworthy drug, istradefylline is proven to be extremely selective and used as an oral active adenosine A_{2A} receptor antagonist (Chen et al., 2007; Murugesan et al., 2025) against sclerosis, spinal cord injuries, myelopathy (Kutryb-Zając et al., 2023) and various cancers(da Silva et al., 2023). Istradefylline is a xanthine derivative and the only FDA-approved drug for the treatment of Parkinson's disease which has emerged as an adjunctive therapy.

As the CK1δ and CK1ε isoform possess higher conservation and affinity at their catalytic domain (Gross and Anderson, 1998; Du et al., 2021), the present work is initially focused in assessing the binding efficacy of riluzole with CK isoforms (α, β, γ1, γ2, γ3, δ, and ε) and istradefylline with adenosine A_{2A} receptor through the molecular interaction and docking studies. Based on the efficient interaction of these two FDA-approved drugs with their target site, they were further experimentally validated to investigate the GBM cell death through various *in vitro* experiments. Overall, CK1δ and adenosine A_{2A} receptor targeting FDA approved drugs were repurposed to investigate their efficacy against GBM cell growth and proliferation.

2. Methods

2.1. Chemicals, enzymes and reagents

The human glioblastoma cell lines LN229, SNB19 (Xu et al., 1998 Attardi et al., 2004) (gifted by Prof. Maria Stella Carro, University Medical Center Freiburg, Germany); Human brain astrocytoma cell line, 1321N1 (Tonazzini et al., 2010) 1321N1 (Istituto Zooprofilattico, Brescia, Italy); Mouse embryonic fibroblast cells (MEF) (gifted by Prof.

Table 1
Recent examples of FDA approved drugs for GBM treatment in different phases of clinical trials representing their targe and its corresponding effect. The data was retrieved from ClinicalTrials.gov, Accessed Mar 7, 2025.

Treatment	Clinical trials phase	Type	Target	Effect
CAR T	phase I	CAR cells	CARv3-TEAM-E EGFRvIII interleukin (IL)-13Rα2 GD2	enhance or trigger an immune response
SurVaxM	phase II	synthetic conjugated vaccine	survivin, inhibitor of apoptosis	
DCVax-L	phase III	dendritic cell vaccine	tumor antigens (incl. EGFRvIII)	
MV-CEA	phase I	oncolytic measles virus	Immune system	
CAN-3110	phase I	oncolytic herpes simplex virus	Immune system	
Depatuxizumab mafodotin	phase III	monoclonal antibody	EGFR	delivers temozolomide once endocytosed
Bevacizumab	FDA approved in 2009		VEGF	blocks proliferation
Trotabresib	phase I	small molecule	bromodomain and extraterminal proteins	
Temozolomide	FDA approved in 2005		DNA	DNA crosslinking
Carmustine	FDA approved in 1976, in 1996 as Gliadel Wafer and in 2003 as wafer implant			
Lomustine	FDA approved in 1976			
Hypofractionated radiotherapy	phase II	Approach (reduces treatment duration)	DNA	improves quality of life
Stereotactic radiosurgery	phase I/II	surgery	Tumor area	minimizes surgical invasion
Optune, tumor treating fields device	FDA approved in 2015	alternating electric fields at 200 kHz	tumor treating fields (TTF) device	disrupts tumor cell division

Pasi Kallio, Faculty of Medicine and Health Technology, Tampere) were cultured and maintained in Dulbecco's Modified Eagle Medium (DMEM) (Cat. No. D5796-500 ML, Sigma-Aldrich, St. Louis, MO, United States). The cell lines free of mycoplasma were used for all the in-vitro analyses. The following chemicals, enzymes, and reagents were purchased from the following respective companies: Dulbecco's Modified Eagle Medium (Cat. No. D5796-500 ML, Sigma-Aldrich, St. Louis, MO, United States); fetal bovine serum (Cat. No. S181H, Biowest, Nuaillé, France); Streptomycin and Penicillin (Cat. No. P4333-100 ML, Sigma-Aldrich, St. Louis, MO, United States); Riluzole (Merck, Cat. No. R116); Istradefylline (Merck, Cat. No. SML0422): dimethyl sulphoxide (Cat. No. D5796-500 ML, Sigma-Aldrich, St. Louis, MO, United States); propidium iodide (PI) (Thermo Fisher Scientific, Waltham, MA, USA).

2.2. Molecular docking

The molecular docking of six Casein kinase isoforms with riluzole was carried out using AutoDock Vina to explore their binding interactions (Trott and Olson, 2010). The Protein Data Bank (PDB) structures of casein kinase isoforms (PDB ID: 3UYS, 5FQD, 4HNI, 2CMW, 2C47, and 2CHL) and Human adenosine A_{2A} receptor (PDB ID: 3EML) were acquired from the Protein Data Bank (Trott and Olson, 2010). In order to make a comparative study of riluzole and istradefylline is docked with Casein kinase delta and adenosine A_{2A} receptor, respectively. These structures have been thoroughly examined, and the missing residues were modeled by homology modeling (Pettersen et al., 2004). The protein structure was optimized for each isoform and adenosine A_{2A} receptor by removal of water molecules, addition of hydroxyl groups, and Gasteiger charges allocation. The co-crystallized ligand was used to identify the catalytic or allosteric active site of all the examined isoforms and adenosine A_{2A} receptor. The spherical grid box with a 10 Å radius was centered on the active site residue to conduct rigid docking of the ligands.

Riluzole and istradefylline, the ligand utilized in the investigation was obtained from the PubChem database (PubChem CID: 5070 & 5311037) (Bolton et al., 2011). All Gasteiger charges were allocated, and the structure was transformed into PDBQT format as necessitated for the utilization in the AutoDock Vina application (Morris et al., 2009). The docking simulation was organized according to the prepared protein and ligand files (Casein kinase isoforms with riluzole and istradefylline; adenosine A_{2A} receptor with riluzole and istradefylline). The exhaustiveness parameter was set to 8 to ensure a thorough search of possible binding conformations, and thus, the AutoDock Vina generated multiple binding modes for each isoform-ligand complex (Trott and Olson, 2010). Subsequently, we have analyzed the various types of binding to ascertain the binding affinity of ligands with all casein kinase isoforms. Molecular docking investigations found that conformation exhibiting the lowest binding energy was deemed the most advantageous. Post-docking analysis, similar to the initial docking phase, was conducted using AutoDockTools and PyMOL to match the binding conformation of ligands with the active site residues of the particular isoform via hydrogen bonding and hydrophobic interactions. To understand the ligands binding and orientation to the protein, the binding pose and orientation of the chemical were examined in greater depth.

2.3. Molecular dynamics simulations

Molecular dynamics (MD) simulation of Casein kinase 1 delta (CSNK1D) with istradefylline and riluzole and adenosine A_{2A} receptor with istradefylline and riluzole were conducted using GROMACS to examine the structural characteristics of the protein-ligand complex and its dynamic properties (Van Der Spoel et al., 2005). The protein-ligand complex structures were acquired from the docking results. Molecular dynamics simulations were conducted, and the structures were energy-minimized. The ligand was constructed and optimized, and the protein-ligand complex was parameterized using the AMBER force field (Hornak et al., 2006).

The protein-ligand complex was situated in a cubic box filled with TIP3P (transferable intermolecular potential with 3 points) water molecules, employing periodic boundary conditions to simulate the aqueous environment (Price and Brooks, 2004) Sodium and chloride ions were included to equilibrate the charge and attain a physiological ionic strength of 0.15 M for the system. Energy minimization was conducted to remove steric hindrances and unfavorable interactions inside the system, hence yielding an optimal initial shape. The equilibration process was thorough, conducted in two phases: initially under NVT conditions for 100 ps to stabilize temperature, followed by NPT conditions for an additional 100 ps to stabilize pressure. During these processes, the protein backbone was configured to minimize conformational search, while the solvent and ions were let to optimize their positions around the complex, ensuring the most reliable results.

2.4. Cell culture and drug preparation

Glioblastoma cells LN229, SNB19 and Mouse embryonic fibroblast cells (MEF) were cultured and maintained in DMEM medium supplemented with 10 % FBS, 0.1 mg/mL Streptomycin, 100 U/mL Penicillin. The cells were cultured as monolayer under appropriate culture conditions in a humidified incubator at 37 °C supplemented with 5 % CO_2 and 95 % humidity. The cells were replenished once in 3 day at a concentration of ~80 % confluency. Riluzole and istradefylline, FDA approved drugs, were dissolved in DMSO to obtain a stock solution of 100 mM and intermediate dilutions were prepared according to the methodology.

2.5. Inhibitory kinetic assay

GBM cells were seeded in DMEM medium in 12 well plates at a concentration of 3×10^5 cells/well. Dose-dependent kinetics analysis was performed using varying concentration of riluzole and istradefylline (10 μM, 25 μM, 50 μM, 100 μM and 150 μM) after 48 h of incubation under suitable cell culture condition. To evaluate the drug's effectiveness in preventing cell division, it must be incubated for at least the period of one complete cell cycle. Since the doubling time for LN229 is 24 h(Weller et al., 1998) and SNB19 is 24 h(Gross et al., 1988), we have chosen 48 h treatment as optimal for all the in-vitro studies performed. The cell viability was calculated as described previously using trypan blue staining method. Dose-response curves were calculated by non-linear regression analysis and half maximal inhibitory concentration (IC_{50}) specific for each cell line and compounds were calculated using GraphPad Prism 10.0.

2.6. In-vitro cytotoxicity assay

A total of 7×10^5 LN229 and SNB19 cells were seeded in 6-well cell culture plates and incubated at 37 °C in a humidified atmosphere with 5 % CO_2. At 60–70 % confluence, the GBM cells were treated with 150 μM concentration of riluzole and istradefylline and incubated for 48 h at appropriate cell culture conditions. DMSO (0.1 %) was used as a negative control. The cells were further treated with fresh cell culture medium to stop the reaction and collected by centrifugation at 3000 rpm for 5 min. The number of live and dead cells were counted by trypan blue staining using Countess II FL Automated Cell Counter (Thermo Fisher Scientific, Carlsbad, CA, USA). Similar procedure was performed on MEF cells to investigate the effect of riluzole and istradefylline in non-cancerous cells at 150 μM concentration. The % of growth inhibition was calculated using equation (1)

$$Inhibition\ (\%) = \frac{Mean\ of\ untreated\ cells\ (DMSO\ control) - Mean\ of\ treated\ cells}{Mean\ of\ untreated\ cells\ (DMSO\ control)} x100 \quad (1)$$

2.7. Cell cycle assay

For cell cycle analysis using Fluorescence-activated cell sorting (FACS), LN229 and SNB19 cells were plated in 12-well pate at 3×10^5 cells/well in DMEM medium supplemented with 10 % FBS. At 60–80 % confluency, the cells were treated with 100 μM of riluzole and istradefylline, and the concentration was chosen based on the 50 % cell death obtained in the initial kinetics studies. DMSO (0.1 %) was also used as a negative control. After 48 h of treatment, the cells were collected by trypsinization, resuspended in 0.5 mL ice cold PBS and fixed by adding 70 % ice cold ethanol for 30 min at 4 °C. The cells were subjected to FACS analysis after suspending the cells in 200 μL PBS containing 20 μg/mL propidium iodide (PI), 0.2 mg/mL RNase and 0.1 % Triton X-100 and incubated for 30 min at 37 °C. The cells were washed again with PBS and subjected to FACS analysis. The cells at different phases of growth were measured using flow cytometer (CUBE 8, SYSMEX, Kobe, Japan) and the generated data were analyzed by FlowJo 10.8.1 software.

2.8. Apoptosis assay by flow cytometry

The apoptosis assay was performed using Dead cell apoptosis kit with Annexin V-Alexa Fluor™ 488 and PI (Ref. V13245, ThermoFisher Scientific, Waltham, MA, USA) following the manufacturer's protocol. LN229 and SNB19 cells were seeded at a density of 3×10^5 cells/well and treated with 100 μM of riluzole and istradefylline for 48 h at 60–80 % confluence. After treatment, the cells were collected, trypsinized, centrifuged, and the cell pellets were washed and resuspended using ice cold PBS. Finally, 100 μL of cell suspension were fixed with 5 μL of FITC conjugated Annexin V, 1 μL of 100 μg/mL PI, and incubated for 15 min at room temperature (Karjalainen et al., 2017). Following the incubation period, the fluorescence was measured using flow cytometry (CUBE 8, SYSMEX, Kobe, Japan), at 488 nm excitation/532 nm and 575 nm emission detection. All the data obtained were analyzed with FlowJo 10.8.1.

2.9. Effect of riluzole and istradefylline on spheroids grown in 3D environment

Astrocytoma cell line, 1321N1 cell line was seeded at a density of 750 cells/well and incubated for 6 days at 37 °C with 5 % CO_2, in cell repellent U bottom 96 well CELLSTAR® plates (Reference No.650970 Lot.E231035S)(Marucci et al., 2011). Quality of the cells were primarily selected based on agarose-based protocol for other solid tumors (Friedrich et al., 2009). Spheroids with suitable diameter above 500 μm after 6 days of culture were selected for the analysis, thus mimicking tumor environment. Spheroids with lowest inter-well variability were selected for drug treatment. For the comparative experiment, 10,000 cells per well was seeded in traditional TC-threated flat bottom transparent 96-well plate. Both 2D and 3D 1321N1 cell cultures were treated with variable concentrations of riluzole and istradefylline (25, 50, 100, 150, 200 and 300 μM) for 24 h. The 96 well plate with spheroids was divided into two parts, where one set was used to study the 3D spheroids with The CellTiter 96® AQueous One Solution Cell Proliferation Assay alongside with the 2D culture, while the other part was used for the size-treatment proliferation study. The effects of riluzole on spheroid cell viability was assessed at concentrations of 25, 50, 100, 150, 200, and 300 μM, revealing no effect from 25 to 150 μM, while 300 μM exhibited greater cytotoxicity compared to 200 μM. Hence, an effective dose of 300 μM was used for the 3D spheroid size treatment study over 18 days. The long-term ability of the drugs to inhibit the proliferation of solid tumors was confirmed by monitoring the spheroid proliferation until ten days after the treatment. Spheroid size and volume were analyzed using SpheroidSizer – a MATLAB-based and open-source software (Chen et al., 2014).

2.10. Statistical analysis

All the experiments were performed in replicates ($n \geq 5$). Data were statistically analyzed using ANOVA with Dunnett's test. Data are expressed as mean ± SE, and $p < 0.05$ and $p < 0.001$ was interpreted as statistically significant and represented as * and ** respectively.

Table 2
Binding interactions of two ligands, istradefylline and riluzole, casein kinase isoforms (PDB ID: 3UYS, 5FQD, 4HNI, 2CMW, 2C47, and 2CHL) and Human A_{2A} Adenosine Receptor (PDB ID: 3EML). The table includes the isoform names, corresponding PDB IDs, key amino acid interactions with ligands, and binding energies (kcal/mol), highlighting the ligand affinities for specific targets.

Isoforms	PDB ID	Ligand	Key Residues	Binding Energy (Kcal/mol)
Human A_{2A} Adenosine Receptor	3EML	Istradefylline	CYS245, SER277, ASP52, PRO285, SER281, ASN280, ASN24, VAL282, VAL283, ILE238, PHE242, ASN284, LEU95, LEU241, LEU48, SER91, ALA51, LEU87, THR88, VAL55, VAL84, ILE60, ALA59, HIS278, TRP246	−9.88
Human A_{2A} Adenosine Receptor	3EML	Riluzole	PHE168, TYR271, SER67, ILE66, ILE274, TYR9, ALA63, TRP246, LEU85, LEU249, HIS278, SER277, VAL84	−6.37
CSNK1D	3UYS	Istradefylline	ILE148, LEU135, ASP132, ASP91, LEU84, LEU85, LEU138, LEU85, GLY86, PRO87, LYS14	−6.13
CSNK1D	3UYS	Riluzole	THR184, GLY175, THR174, GLN190, ASP195, HIS126, ILE125, SER191, ARG127, ASP194, ASP128, THR176, TYR179, LYS130, VAL129, TYR179, ALA180	−9.02
CSNK1A1	5FQD	Riluzole		−7.85
CSNK1E	4HNI	Riluzole		−7.74
CSNK1G1	2CMW	Riluzole		−7.56
CSNK1G2	2C47	Riluzole		−7.25
CSNK1G3	2CHL	Riluzole		−6.97

3. Results

3.1. Molecular docking

Molecular docking was performed for the two ligands istradefylline and riluzole to investigate the binding properties favoring thermodynamics of biological systems. Table 2 delineates the binding interactions of the two ligands, istradefylline and riluzole, with different protein isoforms representing their corresponding PDB IDs, key amino acid residues involved in interactions, and binding energies (Kcal/mol). The binding energies varies from −6.13 to −9.88 kcal/mol. Particularly, istradefylline showed highest binding affinity (−9.88 kcal/mol) for the Human adenosine A_{2A} receptor (PDB ID: 3EML), surpassing riluzole, which binds at a lower energy of −6.37 kcal/mol to the same receptor. In contrast, riluzole exhibits a strong interaction with the CSNK1D isoform (PDB ID: 3UYS), demonstrating a highest binding energy of −9.02 kcal/mol, though istradefylline has a least binding energy of −6.13 kcal/mol. Riluzole also presented a moderate binding affinities for the other isoforms of CSNK1 family, with the highest affinity for CSNK1A1 (PDB ID: 5FQD; −7.85 kcal/mol), followed by CSNK1E (PDB ID: 4HNI; −7.74 kcal/mol) and CSNK1G (PDB IDs: 2CMW, 2C47, and 2CH; exhibiting −7.56, −7.25, and −6.97 kcal/mol, respectively).

Fig. 1A represents the bound form of the adenosine A_{2A} receptor with its ligands, istradefylline and riluzole, featuring both 3D and 2D representations of the binding modes. Specifically, in the adenosine A_{2A} receptor -istradefylline complex (**top**), the binding score (−) 9.88 kcal/mol computed from inter -residue interactions including Asp 52, Asn 280, and Ser 277 leading to intermolecular contacts through hydrogen

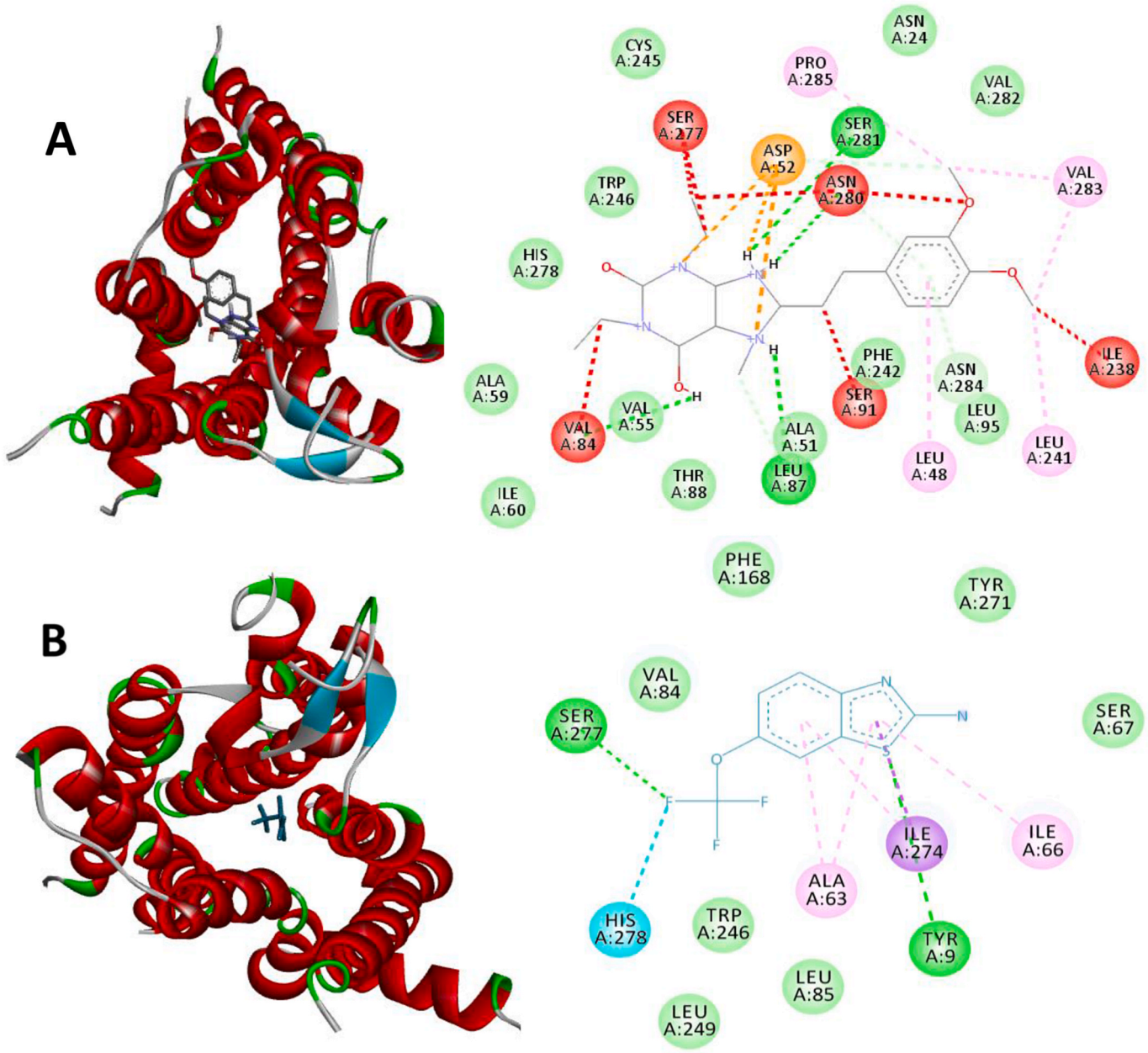

Fig. 1. Molecular interactions of the A_{2A} adenosine receptor with ligands, istradefylline and riluzole. (A) The top panel depicts the binding of istradefylline, highlighting key interactions with residues such as Asp52, Asn280, and Ser277. (B) The bottom panel represents riluzole's binding, with interactions involving residues including Tyr271, Ser277, and Ile274. 3D structures show the ligand positions within the receptor pocket, while 2D diagrams detail the interaction networks, including hydrogen bonds, hydrophobic contacts, and π-π stacking.

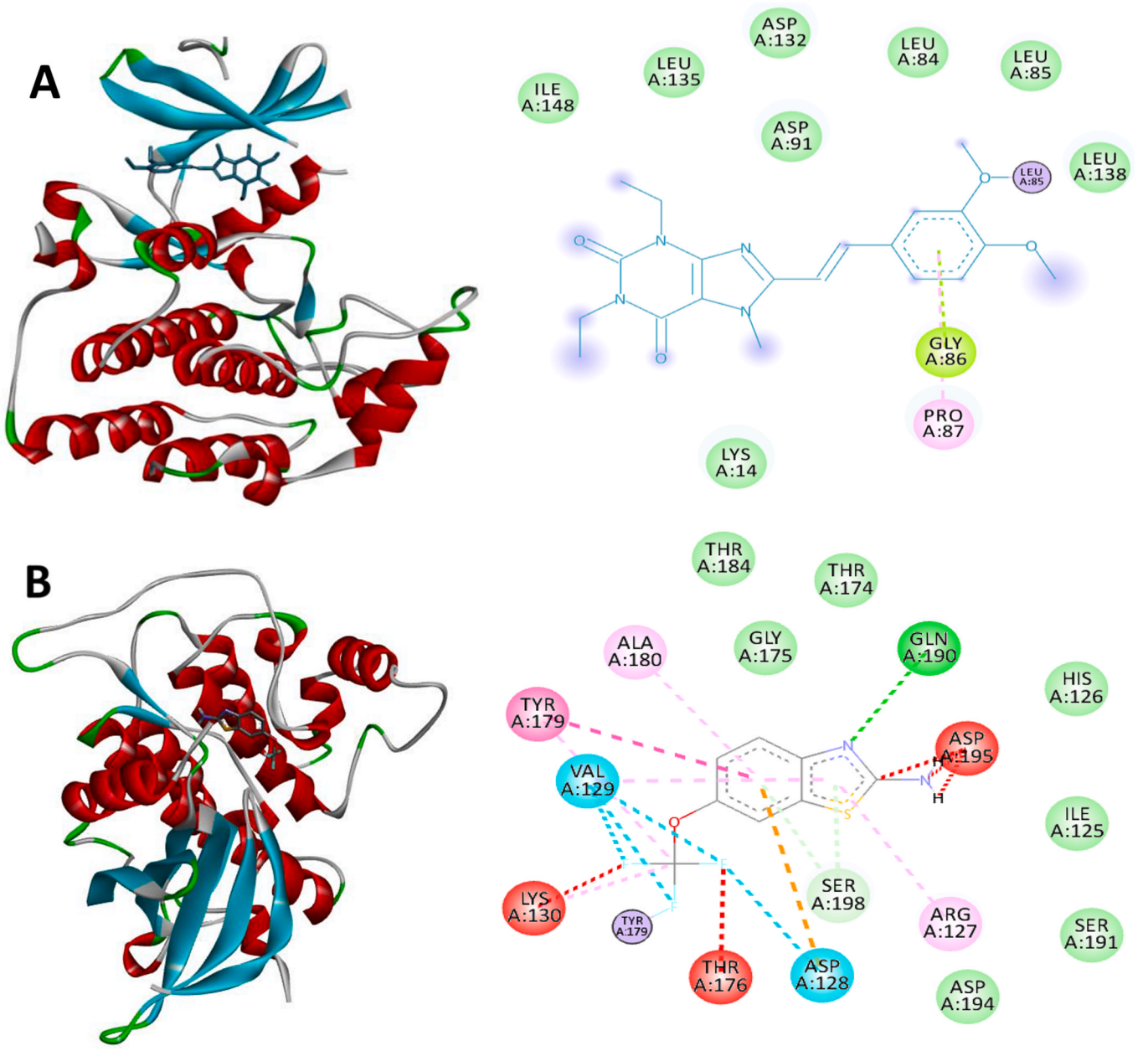

Fig. 2. Molecular interactions of Casein Kinase Delta (CSNK1D) with ligands, istradefylline and riluzole. **(A)** The top left figure displays 3D interaction, and the right figure shows 2D binding of istradefylline with key residues like Gly86, Asp91, and Leu135. **(B)** The bottom left picture shows 3D interaction and the right shows 2D binding of riluzole highlighting interactions with residues like Asp128, Tyr179, and Ser198. The 3D structures depict ligand positioning within the active site, while the 2D diagrams details the interaction networks, including hydrogen bonds and hydrophobic contacts.

bonding, hydrophobic interactions, and π-π stacking, which contributes to perfect fitting inside the active site of the receptor. Likewise, the comparative docking between adenosine A_{2A} receptor -riluzole complex (**bottom**) revealed that riluzole interacts with Tyr9 which further displayed hydrogen bonding between Glu 271-Ser277 and Ala 63-Ile 274, exhibiting lower binding energy −6.37 kcal/mol inferior to istradefylline, which was also represented in the subdued interaction profile in the 2D representation. 3D model illustrates the position of riluzole within the receptor pocket, however additional interactions appear at the receptor pocket as reported with istradefylline (Fig. 1B).

Further, molecular interaction was also analyzed between Casein Kinase Delta (CSNK1D) with istradefylline and riluzole. Fig. 2A illustrates the 3D and 2D interactions between CSNK1D and istradefylline, revealing two notable interactions: a hydrogen bond with Gly86 and Asp91, and a hydrophobic bond with Leu135 and Ile148, resulting in an energy score of −6.13 kcal/mol. Fig. 2B illustrates the three-dimensional and two-dimensional interaction between CSNK1D and riluzole, highlighting relative binding through hydrogen bonds with residues Asp128, Tyr179, and Ser198, and hydrophobic interactions with Gly175 and Thr176. Thus, CSNK1D-riluzole exhibits greater level of interaction, likely attributable to its denser projection than the istradefylline, with a good binding score of −9.02 kcal/mol.

3.2. Molecular dynamics

In the current study, the Molecular Dynamics Simulations (MDS), was performed for 100 ns to identify the binding interactions, dynamics and flexibility of riluzole and istradefylline when binding to the casein kinase Delta and A_{2A} human adenosine receptor (hadenosine A_{2A} receptor), respectively. The root mean square deviation (RMSD) was

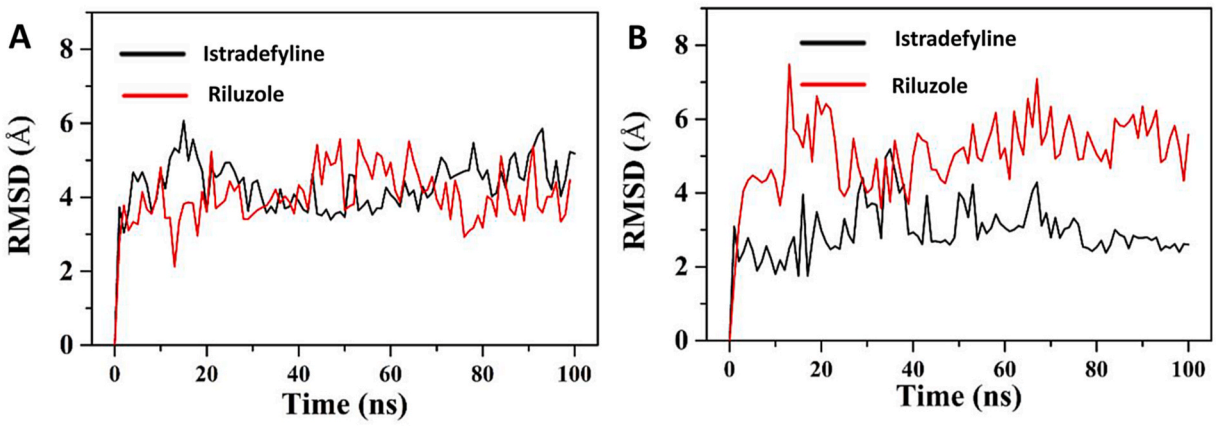

Fig. 3. The root-mean-square deviation (RMSD) of the protein backbone for two protein-ligand complexes during 100 ns (ns) of molecular dynamics simulations. **(A)** The RMSD profiles for the adenosine A2A receptor bound with istradefylline (black) and riluzole (red), **(B)** The RMSD profiles for Casein Kinase Delta bound with istradefylline (black) and riluzole (red). RMSD, measured in Ångströms (Å), indicates the stability of the protein-ligand complexes over the time. The structures of istradefylline and riluzole are shown alongside the corresponding RMSD plots for reference.

assessed from the trajectory data collected over the 100-ns period, in order to investigate the biomolecular system's structure stability, as it analyses the positioning of protein backbone atoms relative to the original reference. Panel A of Fig. 3A displays the RMSD curve for the adenosine A_{2A} receptor complexed with istradefylline (**black**) and riluzole (**red**). Upon comparing the dynamic features of the two ligands, distinct behaviors emerge with istradefylline, which exhibits very low variance in RMSD when compared to riluzole, suggesting a robust engagement with the receptor. This tendency is notably more pronounced for riluzole, suggesting that the protein may exhibit greater conformational freedom or reduced binding stability for this drug.

Panel B from Fig. 3 illustrates the RMSD patterns for Casein Kinase Delta in conjunction with the identical ligands. As already shown in Fig. 3A, istradefylline (**black**) has superior binding stability with reduced RMSD values, while riluzole (**red**) shows heightened variability, particularly after 40 ns with Casein Kinase Delta. This suggests that istradefylline aligns more effectively with the active site pocket of Casein Kinase Delta compared to riluzole. Thus, the more robust or frequent contacts between istradefylline and Casein Kinase Delta indicate that the resulting complex is comparatively stable. The structures of both ligands are depicted alongside the plots to illustrate their distinct molecular configurations. Due to its xanthine-based structure,

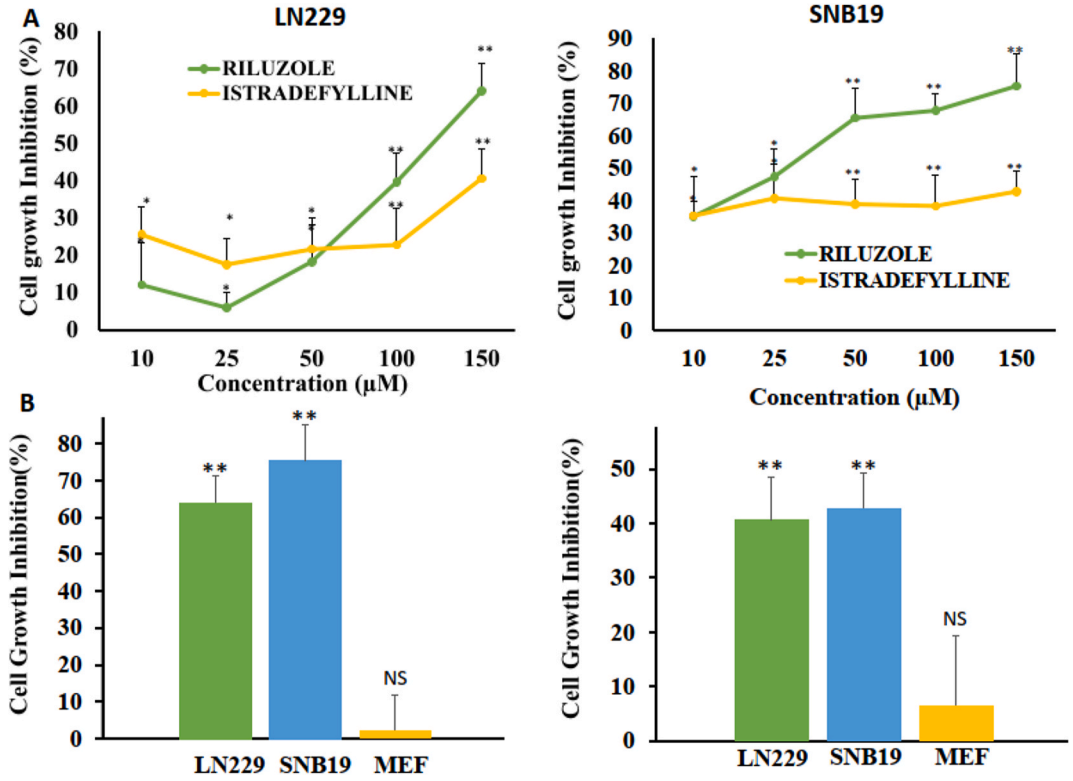

Fig. 4. Growth inhibitory effect of riluzole and istradefylline. **(A)** Dose Responsive curve of riluzole and istradefylline in LN229 and SNB19 cells at varying concentrations including 10, 25, 50, 100, and 150 μM at 48 h of treatment. **(B)** % of growth inhibition by riluzole and istradefylline in LN229, SNB19 and MEF cells at 150 μM concentration. All data were represented as mean ± standard deviation (n = 6). * represent statistically significant differences between the riluzole Vs control, istradefylline Vs control. *$p < 0.05$; **$p < 0.001$; and ns $p > 0.05$.

istradefylline may engage in specific hydrophilic interactions, such as hydrogen bonding or stacking interactions, hence providing stability. Riluzole contains a benzothiazole moiety and two trifluoromethyl groups, which may provide flexibility, either sterically or electronically. The aggregate data illustrates the distinct binding properties of these ligands with two different protein partners, with istradefylline demonstrating consistent interactions with both the receptors. This research aids in understanding ligand selectivity and is especially pertinent for the systematic development of drugs targeting these proteins. Furthermore, we have performed the biological evaluation to investigate the GBM cell growth inhibition through various in-vitro experiments.

3.3. In-vitro antiproliferative activity of riluzole and istradefylline

The riluzole and istradefylline were screened for their anti-proliferative activities against GBM cell lines, LN229 and SNB19. Dose response of these two FDA approved drugs was established to determine the correlation between cell growth inhibition and drug concentration. The initial cytotoxicity assay was performed with 10 μM of istradefylline and riluzole, which showed the cell death ranging between 10 and 30 % for both cell lines. Hence, we further screened the cytotoxicity effect with higher concentrations of 10 μM, 25 μM, 50 μM, 100 μM and 150 μM for both drugs at 48 h. Results depicted in Fig. 4A indicated that riluzole reduced both LN229 (64 %) and SNB19 (75 %) cell proliferation significantly ($p < 0.001$) in a dose dependent manner more effectively than istradefylline, which was about 40 % even at 150 μM concentration in both the cell lines. The percentage of growth inhibition by riluzole increased gradually as the concentration increases. Riluzole had an IC_{50} concentration of 121.47 μM and 34.89 μM, while istradefylline had a higher IC_{50} concentration of 374.56 μM and 399.72 μM for LN229 and SNB19, respectively. Hence, the anti-proliferative activity of istradefylline is regarded minimal due to its higher IC_{50} value of >100 μmol/L, which is above the therapeutically accessible concentration. It was observed that riluzole inhibits 24 % higher LN229 cell growth with 36 % in SNB19 cells than istradefylline. While the higher concentration of 150 μM exhibited only ~70 % cell death in both cell lines, we also tested whether the same concentration would be toxic to non-cancerous cells, MEF and the data revealed least cytotoxicity effect of about 2.2 % and 6.4 % of cell death for riluzole and istradefylline, respectively. The effect of these drugs in non-cancerous MEF cells reflected the least toxicity revealing their potential anti-cancerous activity (Fig. 4B**).**

3.4. Evaluation of cell cycle arrest and apoptotic mechanisms of the drugs

The effect of riluzole and istradefylline on cell cycle progression of GBM cells was assessed by flow cytometry. LN229 and SNB19 cells were treated with 100 μM of the drugs with 0.1 % of DMSO as a negative control for 48 h stained with Annexin V-Alexa Fluor™ 488 and Propidium Iodide (PI) and analyzed using the histogram (Fig. 5A) obtained by flow cytometry. Fig. 5B showed the presence of ~10 % of cells at S phase in riluzole than DMSO treated LN229 and SNB19 cell line. Istradefylline treated SNB19 cells demonstrated a high level of G1 phase with 6 % of cells than DMSO, however no significant arrest in LN229 cells.

To further analyze the GBM cells for their apoptosis or necrosis properties, riluzole and istradefylline treated GBM cells were stained with Annexin V/PI double staining. Annexin V represents the cells entering apoptotic phase by binding with the phosphatidylserine in cell membrane, whereas PI represents necrotic cells by staining the DNA once the cells disintegrate. The cells were subsequently sorted by flow cytometry, which revealed that riluzole treatment caused 23.3 % and 60.1 % *($p < 0.001$)* of LN229 and SNB19 cells to enter the early apoptotic phase, whereas 9.1 % and 16.2 % of cells entered the necrotic phase, respectively. Istradefylline treatment triggered early apoptosis in 9.34 % and 17.4 % of LN229 and SNB19 cells, respectively, with less than 10 % of necrotic cells in both cell lines (Fig. 5C). Thus, riluzole induced early apoptosis of GBM cells better than istradefylline, thus inducing programmed cell death in GBM cells.

3.5. Antiproliferative effect of FDA-drugs in 2D monolayer and 3D spheroid model

The effect of riluzole and istradefylline on 3D spheroid model was investigated to mimic the ability of the anti-proliferative effect of the FDA drugs in the tumor environment in-vivo. Hence, a spheroid assay was performed to evaluate the impact of both drugs on the spheroid size, volume, and shape of GBM spheroids, all of which are considered critical factors for cancer cell survival. We developed 3D spheroids using 1321N1 cells in an appropriate cell culture environment (Marucci et al., 2011), and the 3D spheroids with an average diameter of 678 μm and eccentricity of 0.37 were developed and used for further investigation. Before the drug treatment, the spheroids were assessed for their uniformity and those cells with lower variability were selected for further analysis.

The spheroids were treated with 300 μM riluzole, and 0.05 % SDS (positive control) for 18 days (Fig. 6A). The phase-contrast microscopic image showed a significant reduction in the volume upon treatment with 300 μM riluzole from day 9. Likewise, 2D cell viability assay was also performed which showed significant decrease in the % of viability of 1321N1 cells treated with varied concentrations of riluzole and istradefylline (25, 50, 100, 150, 200 and 300 μM). A similar pattern in viability (%) was seen for both FDA drugs up to 300 μM concentration, with riluzole significantly decreasing to 40 % at 300 μM (Fig. 6B). Correspondingly, in 3D environment, the % of viability was reduced to 40 % in riluzole with just 12 % with istradefylline treatment (Fig. 6C). Thus, when compared to 2D viability test, it was considered unique and promising, since the potency of common drugs like cisplatin is usually decreased against spheroids compared to that against monolayers of the same cell line (Melissaridou et al., 2019). This reflects that CK1 isoform δ inhibitors and riluzole specifically and potentially able to surpass the factors of the natural tumor microenvironment such as protective extracellular matrix, cell differentiation, and reach the inner layers of cells in the structure of solid tumors.

Nonetheless, istradefylline was not used for the further comparative spheroid analysis, due to its least potential bioavailability during the spheroid treatment when compared with riluzole. Istradefylline precipitated into a feather-like spiky structure even at the least concentration of 25 μM, which makes it difficult to analyze the long-term post-treatment morphological studies. Hence, riluzole alone was selected for further spheroid treatment, and the release of the drug in the culture environment was enhanced by adding 0.05 % of SDS. After 6 days of monolayer culture, the 3D spheroids were treated with riluzole and the long-term ability to inhibit the proliferation of solid tumors was confirmed by monitoring spheroid proliferation for 10 days after treatment, when compared to non-treated samples. Results showed that riluzole was able to significantly reduce the growth rate of spheroids over the days and completely stopped the proliferation at 300 μM concentration at 15 days. The spheroid volume (mm^3) was significantly reduced to 0.13 mm3 which is equal to the SDS treatment (Fig. 6D). Thus, the overall analysis revealed the possibility of using riluzole as an anti-GBM drug, which could be further investigated for its therapeutic usage.

4. Discussion

Glioblastoma is the most difficult tumor to treat, with a mean survival rate of only 1.2 yrs. No effective treatments after debulking the tumor are available except the use of temozolomide (TMZ) as a chemotherapeutic agent along with radiation therapy. Hence, new therapies and drug combinations essentially need to be developed that can possibly meet the needs of the patient population. However, the use of TMZ makes GBM patients non-responsive due to the high expression of O6-methylguanine methyltransferase (MGMT) (Kitange et al., 2009)

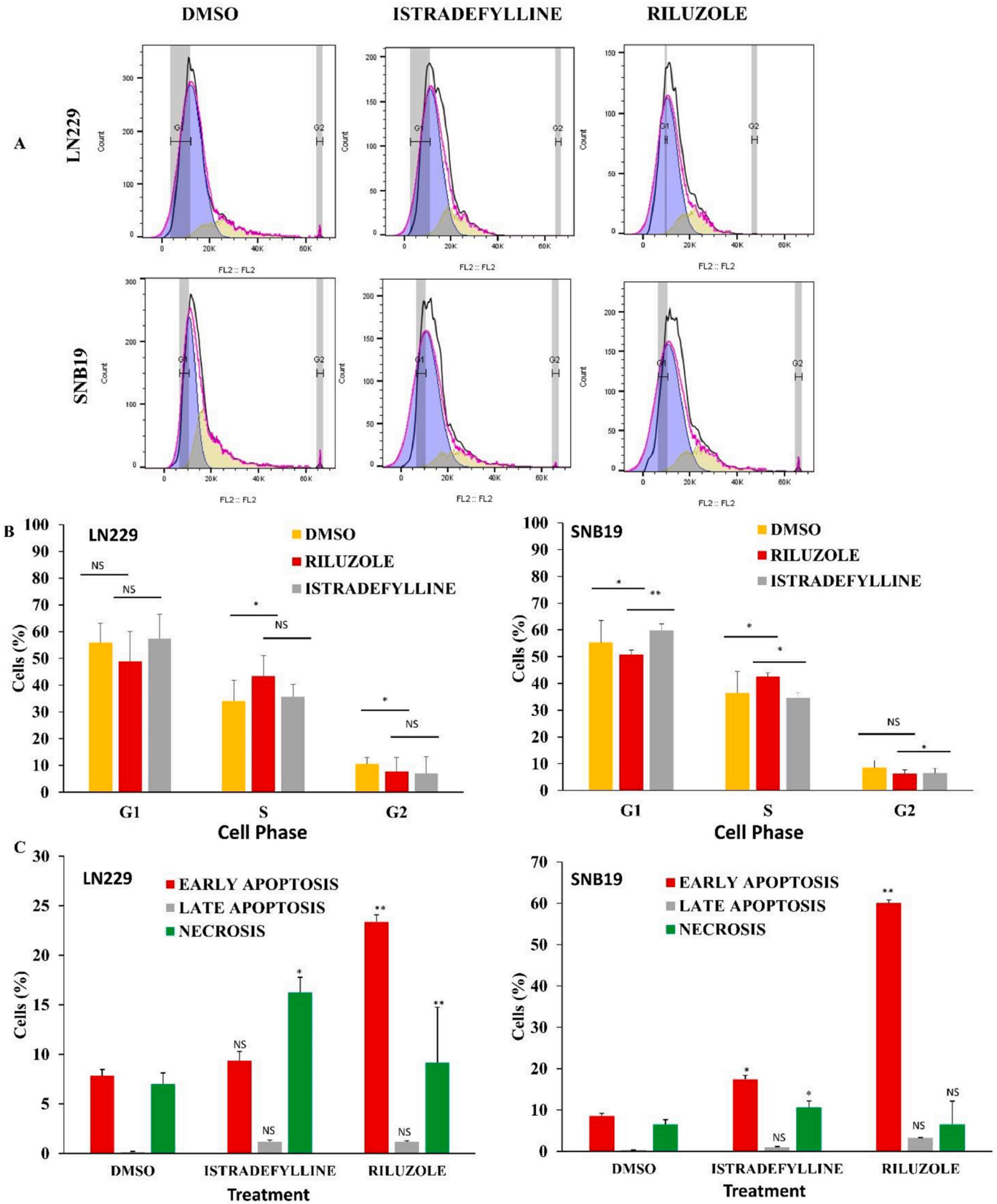

Fig. 5. Effect of riluzole and istradefylline on GBM cell cycle and apoptosis. **(A)** Histogram representing the cells in different phases of cell cycle upon treatment with DMSO (control), istradefylline and Riluzole in both the GBM cell lines; **(B)** Percentage of cells in different phases of cell cycle after treatment with 100 μM of riluzole, istradefylline, DMSO served as a negative control. **(C)** Percentage of cells in representing cells in live cells, early, late apoptosis and necrosis after 48 h of treatment with istradefylline and riluzole. All data were represented as mean ± standard deviation (n = 5). * represent statistically significant differences between the riluzole Vs control, istradefylline Vs control. *$p < 0.05$; **$p < 0.001$; and ns $p > 0.05$.

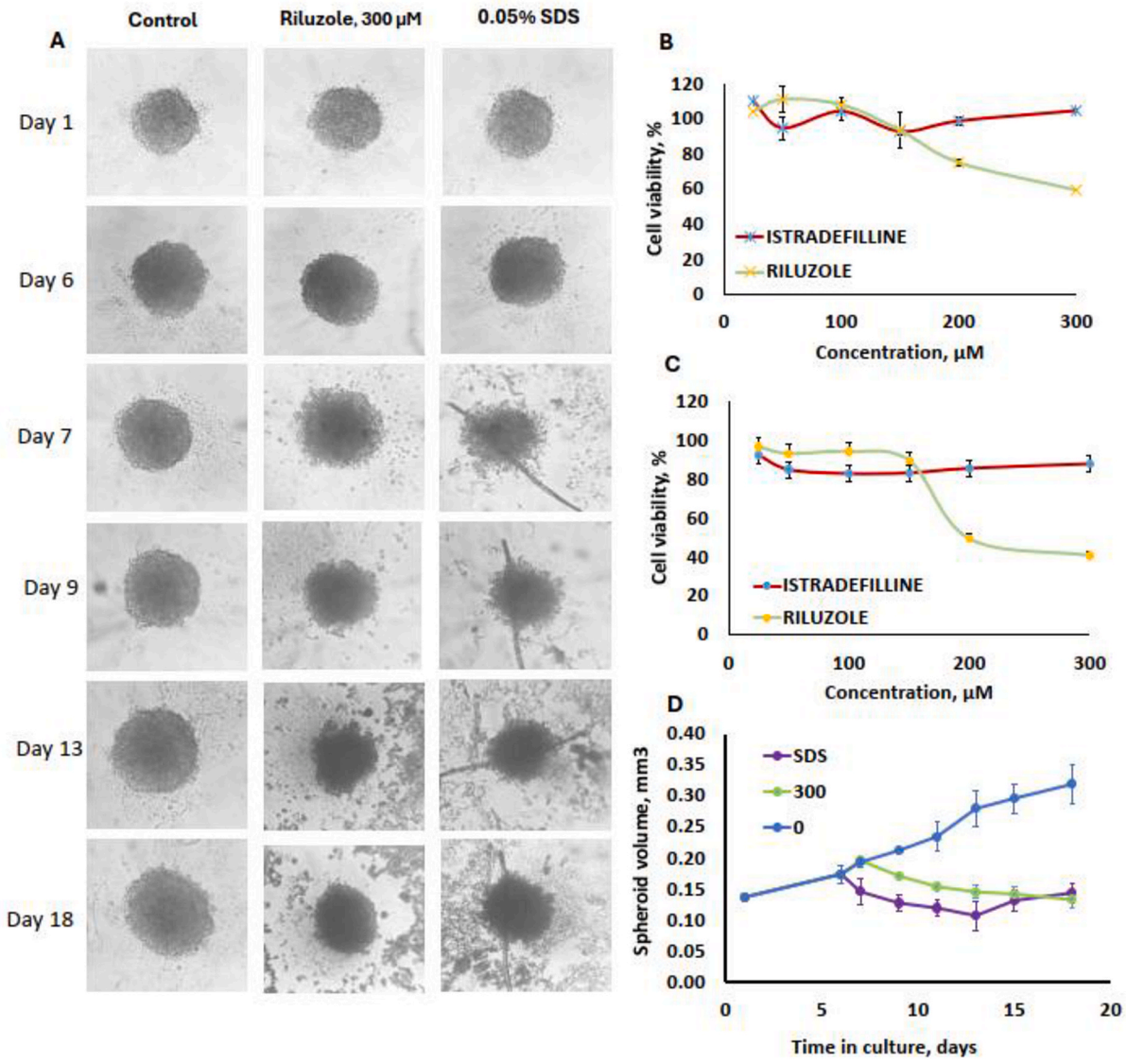

Fig. 6. Effect of riluzole in GBM spheroid growth: (A) Phase contrast microscopic images of long-term spheroid growth with riluzole (300 µM), SDS (0.05 %) as positive control for 18 days of treatment; **(B)** Effect of riluzole and istradefylline on the on 1321N1 cell viability (%) at 25, 50, 100, 150, 200 and 300 µM concentration; **(C)** Effect of riluzole and istradefylline on the spheroid cell viability (%) at 25, 50, 100, 150, 200 and 300 µM concentration; **(D)** Measurement of spheroid volume (mm^3) after treatment with 300 µM of riluzole for 18 days. Mean values and standard deviations of viability and size are based on two interday experiments performed in duplicates for each point. Data on volumes was derived from microphotographs using active contour algorithm (SpheroidSizer, MATLAB).

and significant increase of GBM stem cells leading to resistance to the TMZ (William et al., 2018). As an economical pipeline, repurposing FDA approved drugs could be one possible approach to eliminate the GBM tumor expansion. There are many drugs at various stages of investigation, i.e drugs at clinical trial phase and drugs in pre-clinical testing. Bevacizumab, an FDA approved drug in 2009, with anti-angiogenic properties blocks the vascular endothelial growth factor A (VEGF-A), have shown only moderate clinical benefit against GBM treatment (Vredenburgh et al., 2007; Friedman et al., 2009). Also, another therapeutic approach for recurrent GBM is the tumor-treating fields (TTF) which have received FDA approval delivers low intensity and alternating electric fields to the tumor and inhibits glioma cell proliferation, but only least improvement in the survival of diagnosed GBM patients have been observed (Stupp et al., 2015, 2017). GBM heterogeneity and blood brain barrier are the major key factors for the failure of conventional and targeted therapies. In a similar approach our present work was focused on repurposing FDA approved drugs, riluzole and istradefylline, and the comparative study was performed to identify the potential of the drugs as an inhibitor in GBM signaling pathway.

It was unveiled that riluzole can inhibit glutamatergic communication in the brain, but with least evidence to support the interaction between the drug and ionotropic/metabotropic glutamate receptors or transporters. Protein kinase C (PKC) enzymes play a complex role in growth, survival and invasiveness of GBM. PKC is involved in initiating EGFR ligand release, a significant signaling pathway leading to GBM prognosis. Hence inhibiting classical PKC enzymes may lead to the reduction in GBM proliferation and tumor prognosis by inhibiting EGFR pathway(Geribaldi-Doldán et al., 2021). Targeting protein kinase CK1δ with riluzole, a brain permeant molecule modulates TDP-43 hyperphosphorylation and prevents physiological localization in cytoplasm, thereby inhibiting glutamatergic signaling due to excitatory amino acid transporter-2 (Rosenblum and Trotti, 2017). Riluzole also modulates the immune system in several cancers including human nasopharyngeal carcinoma (Sun et al., 2020), colorectal cancer (Liang et al., 2025) and glioblastoma (Sperling et al., 2017). These findings support the notion that riluzole, as an inhibitor of CK1δ, could serve as a valuable

pharmacological probe in GBM treatment. Similarly, istradefylline function as a strong, and active antagonist of adenosine adenosine A_{2A} receptor, and was approved to be used as adjuvant therapy in adults with Parkinson's disease. The inhibition of adenosine A_{2A} receptor exhibits neuroprotective benefits by mitigating neuroinflammatory processes and diminishing astroglial and microglial activation, thus suggesting its potential for GBM treatment (Lambertucci et al., 2022).

Previously, computational analysis by Bissaro et al. have reported on the stable binding of riluzole with the CK1δ catalytic site of the kinase inhibitors, at Leu85 through the hydrogen bonding. Similarly, in the present analysis, the docking analysis revealed the strong binding of riluzole was observed with the binding pocket of CK1δ catalytic site with better binding score of **-9.02** kcal/mol than istradefylline. Similarly, istradefylline exhibited strong binding with adenosine A_{2A} receptor with the binding score of 9.88 kcal/mol which is better than riluzole, which was also reported by (Wang et al., 2021), which proves the on the biological activity of istradefylline derivatives based on adenine as adenosine A_{2A} receptor antagonists.

It was identified earlier that riluzole can exerts antiproliferative activity against melanoma, breast cancer and prostate cancer (Akamatsu et al., 2009; Yip et al., 2009; Speyer et al., 2012) with more sensitivity for rat glioma (C6)(Lemieszek et al., 2018). Our studies also revealed that riluzole functions better in reducing the GBM cell growth to 64 % in LN229 cells and ~75 % of SNB19 than the istradefylline with less than 40 % reduction in GBM cell growth. The IC_{50} concentration for both the drugs ranges between 34.89 and 399.72 μM, is cell line and compound specific. There are recent studies in which riluzole showed cytotoxicity even at 20 μM concentration against GBM cells, T98G and GL261 and temozolomide are effective at 100 μM concentration (Yamada et al., 2020). Evaluation of drug concentration through in-vitro and in-vivo experiments often reveals IC_{50} concentration that exceeds the maximally tolerated doses administered to cancer patients (Smith and Houghton, 2013). While the IC_{50} concentration of TMZ was lower in in-vitro studies, the clinically exposed dosage to GBM patients' was determined to be 300–400mg/day. These data reveal the poor response of GBM cells even to the currently used FDA approved chemotherapeutic drugs, which may be due to inter and intratumor heterogeneity. Of note, the clinically effective dosage of istradefylline was 20–40 mg/day (Mizuno and Kondo, 2013) whereas riluzole was 100 mg/day (Spencer et al., 2023), indicating their better clinical efficacy than the TMZ. Riluzole and istradefylline being a well-known FDA approved drugs, the present study highlights the comparative analysis on the potential inhibition of GBM cells through the interaction of their target proteins. Also, the present study gives a glimpse of developing variants of riluzole than istradefylline which will have least IC_{50} concentration against the GBM cell lines.

Another important characteristic feature of cancer cells is the uncontrolled cell cycle regulation. We have investigated the role of these drugs in cell cycle regulation that controls and maintain the homeostasis of cell proliferation. Our results revealed that riluzole arrested the cell cycle better than istradefylline, at S phase in the GBM cells and progress the cells mostly to early apoptosis and least level of cells to necrosis. In several studies, it was indicated that riluzole causes G2/M cell cycle arrest in cancer cells. It induced G2/M phase arrest in pancreatic cancer line by decreasing the regulatory protein cyclin-dependent kinase 1 (Beltran-Parrazal and Charles, 2003). It was also found that the effect of riluzole with other therapeutic agents on glioma cell lines have shown synergistic effect on proliferation inhibition, cell cycle arrest and apoptosis induction, through reduced P13K/Akt and MAPK/ERK signaling pathway (Sperling et al., 2017). Therapeutic potential of riluzole was demonstrated to have synergistic anti-GBM effects in conjunction with mTOR inhibitors by inhibiting the activity of cyclin D1 and the c-myc internal ribosome entry site (IRES) leading to reduced translation (Benavides-Serrato et al., 2020b). Based on our findings, riluzole can also be combined with istradefylline and/or the existing chemotherapeutic drug, temozolomide, to enhance the anti-GBM effect.

Overall, from our investigation, it was revealed that riluzole is effective than istradefylline, by inhibiting the CK1δ isoform, inducing GBM cell death and reduces 3D spheroid volume and downregulates the GBM cell death signaling pathway. Further detailed molecular investigation could be performed to unravel the anti-GBM therapeutic potential of riluzole.

5. Conclusion

Based on the comparative screening of the two FDA approved drugs, it was identified that riluzole functions better than istradefylline in reducing the GBM cell growth, inducing apoptosis mediated cell death and reduces the cell growth % in 2D cell culture and 3D spheroid models. Our data concludes that blocking of adenosine A_{2A} receptor downstream signaling protein, CK1 isoform δ with riluzole have greater influence than its upstream signaling blocker, istradefylline. Thus, blockade of adenosine A_{2A} receptor/CK1δ pathway could be considered for developing targeted therapy against GBM. Our research suggests that riluzole can be synergized with istradefylline and/or temozolomide to augment its therapeutic potential as an adjuvant therapy which may be advanced to clinical phase trial. The impact of riluzole may be investigated on other sub-types of GBM for developing personalized medicine.

CRediT authorship contribution statement

Akshaya Murugesan: Writing – review & editing, Writing – original draft, Visualization, Methodology, Formal analysis, Data curation. **Anxo Vila Alonso:** Writing – original draft, Visualization, Validation, Methodology, Formal analysis, Data curation. **Saravanan Konda Mani:** Writing – original draft, Visualization, Methodology, Investigation, Formal analysis, Data curation. **Puja Sarkar:** Writing – original draft, Methodology, Formal analysis, Data curation. **Aleksei Smirnov:** Writing – original draft, Visualization, Methodology, Formal analysis. **Beatrice Francucci:** Validation, Methodology, Formal analysis. **Gabriella Marucci:** Writing – original draft, Supervision, Methodology, Formal analysis. **Michela Buccioni:** Writing – original draft, Visualization, Methodology, Formal analysis. **Kasim S. Abass:** Visualization, Software, Formal analysis. **Chandrabose Sureka:** Writing – review & editing, Visualization. **Olli Yli-Harja:** Writing – review & editing, Funding acquisition. **Meenakshisundaram Kandhavelu:** Writing – review & editing, Writing – original draft, Supervision, Project administration, Investigation, Funding acquisition, Conceptualization.

Declaration of competing interest

The authors declare no competing financial interest.

Acknowledgement

This research was funded by Fondo di Ateneo per la Ricerca Scientifica (University of Camerino), Grant number FPI002003 and Regione Marche, Project 'Tumori Solidi', Grant number FPI532001.

Abbreviation

GBM, Glioblastoma multiforme; CK1δ-Casein kinase 1δ kinase domain; FDA, Food and Drug Administration; PI3K-phosphatidylinositol 3-kinase; pAKT-phosphorylated AKT; PKC-Protein kinase C; GLUT3-reducing glucose transporter 3; MEF-Mouse embryonic fibroblast cells; DMEM-Dulbecco's Modified Eagle Medium; PDB-Protein Data Bank; MD-Molecular dynamics; DMSO-Dimethyl sulfoxide; TMZ-temozolomide.

Data availability

Data will be made available on request.

References

Akamatsu, K., et al., 2009. Riluzole induces apoptotic cell death in human prostate cancer cells via endoplasmic reticulum stress. Anticancer Res. 29 (6), 2195–2204.

Attardi, L.D., de Vries, A., Jacks, T., 2004. Activation of the p53-dependent G1 checkpoint response in mouse embryo fibroblasts depends on the specific DNA damage inducer. Oncogene 23 (4), 973–980. https://doi.org/10.1038/sj.onc.1207026.

Beltran-Parrazal, L., Charles, A., 2003. Riluzole inhibits spontaneous Ca2+ signaling in neuroendocrine cells by activation of K+ channels and inhibition of na+ channels. Br. J. Pharmacol. 140 (5), 881–888. https://doi.org/10.1038/sj.bjp.0705491.

Benavides-Serrato, A., et al., 2020a. Repurposing potential of riluzole as an ITAF inhibitor in mTOR therapy resistant glioblastoma. Int. J. Mol. Sci. 21 (1), 344. https://doi.org/10.3390/ijms21010344.

Benavides-Serrato, A., et al., 2020b. Repurposing potential of riluzole as an ITAF inhibitor in mTOR therapy resistant glioblastoma. Int. J. Mol. Sci. 21 (1), 344. https://doi.org/10.3390/ijms21010344.

Bissaro, M., et al., 2018. Targeting protein kinase CK1δ with riluzole: could it be one of the possible missing bricks to interpret its effect in the treatment of ALS from a molecular point of view? ChemMedChem 13 (24), 2601–2605. https://doi.org/10.1002/cmdc.201800632.

Bolton, E.E., et al., 2011. PubChem3D: a new resource for scientists. J. Cheminf. 3 (1), 32. https://doi.org/10.1186/1758-2946-3-32.

Cantrell, J.N., et al., 2019. Progress toward long-term survivors of glioblastoma. Mayo Clin. Proc. 94 (7), 1278–1286. https://doi.org/10.1016/j.mayocp.2018.11.031.

Chen, J.-F., et al., 2007. Adenosine A2A receptors and brain injury: broad spectrum of neuroprotection, multifaceted actions and “fine tuning” modulation. Prog. Neurobiol. 83 (5), 310–331. https://doi.org/10.1016/j.pneurobio.2007.09.002.

Chen, W., et al., 2014. High-throughput image analysis of tumor spheroids: a user-friendly software application to measure the size of spheroids automatically and accurately. J. Vis. Exp. (89), 51639. https://doi.org/10.3791/51639.

da Silva, J.L.G., et al., 2023. Istradefylline modulates purinergic enzymes and reduces malignancy-associated factors in B16F10 melanoma cells. Purinergic Signal. 19 (4), 633–650. https://doi.org/10.1007/s11302-022-09909-8.

Du, C., et al., 2021. Achieving effective and selective CK1 inhibitors through structure modification. Future Med. Chem. 13 (5), 505–528. https://doi.org/10.4155/fmc-2020-0215.

Fortunato, A., 2017. The role of hERG1 ion channels in epithelial-mesenchymal transition and the capacity of riluzole to reduce cisplatin resistance in colorectal cancer cells. Cell. Oncol. 40 (4), 367–378. https://doi.org/10.1007/s13402-017-0328-6.

Friedman, H.S., et al., 2009. Bevacizumab alone and in combination with irinotecan in recurrent glioblastoma. J. Clin. Oncol. 27 (28), 4733–4740. https://doi.org/10.1200/JCO.2008.19.8721.

Friedrich, J., et al., 2009. Spheroid-based drug screen: considerations and practical approach. Nat. Protoc. 4 (3), 309–324. https://doi.org/10.1038/nprot.2008.226.

Geribaldi-Doldán, N., et al., 2021. Targeting protein kinase C in glioblastoma treatment. Biomedicines 9 (4), 381. https://doi.org/10.3390/biomedicines9040381.

Gross, S.D., Anderson, R.A., 1998. Casein kinase I: Spatial organization and positioning of a multifunctional protein kinase family. Cell. Signal. 10 (10), 699–711. https://doi.org/10.1016/S0898-6568(98)00042-4.

Gross, J.L., et al., 1988. Plasminogen activator and inhibitor activity in human glioma cells and modulation by sodium Butyrate1. Cancer Res. 48 (2), 291–296.

Hernandez, J.J., et al., 2017. Giving Drugs a Second Chance: Overcoming Regulatory and Financial Hurdles in Repurposing Approved Drugs As Cancer Therapeutics. Frontiers in Oncology 7. https://doi.org/10.3389/fonc.2017.00273.

Hornak, V., et al., 2006. Comparison of multiple amber force fields and development of improved protein backbone parameters. Proteins: Struct., Funct., Bioinf. 65 (3), 712–725. https://doi.org/10.1002/prot.21123.

Jacobson, K.A., Ijzerman, A.P., Müller, C.E., 2021. Medicinal chemistry of P2 and adenosine receptors: common scaffolds adapted for multiple targets. Biochem. Pharmacol. 187, 114311. https://doi.org/10.1016/j.bcp.2020.114311.

Karjalainen, A., et al., 2017. Synthesis of phenol-derivatives and biological screening for anticancer activity. Anti Cancer Agents Med. Chem. 17 (12), 1710–1720.

Kast, R.E., et al., 2013. A conceptually new treatment approach for relapsed glioblastoma: coordinated undermining of survival paths with nine repurposed drugs (CUSP9) by the international initiative for accelerated improvement of glioblastoma care. Oncotarget 4 (4), 502–530. https://doi.org/10.18632/oncotarget.969.

Kitange, G.J., et al., 2009. Induction of MGMT expression is associated with temozolomide resistance in glioblastoma xenografts. Neuro Oncol. 11 (3), 281–291. https://doi.org/10.1215/15228517-2008-090.

Kutryb-Zając, B., et al., 2023. Drugs targeting adenosine signaling pathways: a current view. Biomed. Pharmacother. 165, 115184. https://doi.org/10.1016/j.biopha.2023.115184.

Lambertucci, C., et al., 2022. A2A adenosine receptor antagonists and their potential in neurological disorders. Curr. Med. Chem. 29 (28), 4780–4795. https://doi.org/10.2174/0929867329666220218094501.

Lemieszek, M.K., et al., 2018. Riluzole inhibits proliferation, migration and cell cycle progression and induces apoptosis in tumor cells of various origins. Anti Cancer Agents Med. Chem. 18 (4), 565–572. https://doi.org/10.2174/1871520618666180228152713.

Liang, B., et al., 2025. Riluzole enhancing Anti-PD-1 efficacy by activating cGAS/STING signaling in colorectal cancer. Mol. Cancer Therapeut. 24 (1), 131–140. https://doi.org/10.1158/1535-7163.MCT-24-0289.

Ma, X.-L., et al., 2019. CD73 promotes hepatocellular carcinoma progression and metastasis via activating PI3K/AKT signaling by inducing Rap1-mediated membrane localization of P110β and predicts poor prognosis. J. Hematol. Oncol. 12 (1), 37. https://doi.org/10.1186/s13045-019-0724-7.

Marucci, G., et al., 2011. Comparison and optimization of transient transfection methods at human astrocytoma cell line 1321N1. Anal. Biochem. 414 (2), 300–302. https://doi.org/10.1016/j.ab.2011.02.028.

Mehta, M., et al., 2017. Critical review of the addition of tumor treating fields (TTFields) to the existing standard of care for newly diagnosed glioblastoma patients. Crit. Rev. Oncol. Hematol. 111, 60–65. https://doi.org/10.1016/j.critrevonc.2017.01.005.

Melissaridou, S., et al., 2019. The effect of 2D and 3D cell cultures on treatment response, EMT profile and stem cell features in head and neck cancer. Cancer Cell Int. 19 (1), 16. https://doi.org/10.1186/s12935-019-0733-1.

Morris, G.M., et al., 2009. AutoDock4 and AutoDockTools4: automated docking with selective receptor flexibility. J. Comput. Chem. 30 (16), 2785–2791. https://doi.org/10.1002/jcc.21256.

Murugesan, A., et al., 2025. A2A receptor antagonist 4-(2-((6-Amino-9-ethyl-8-(furan-2-yl)-9H-purin-2-yl)amino)ethyl)phenol, a promising adenosine derivative for glioblastoma treatment. Eur. J. Pharmaceut. Sci. 207, 107039. https://doi.org/10.1016/j.ejps.2025.107039.

Mizuno, Y., Kondo, T., 2013. Adenosine A2A receptor antagonist istradefylline reduces daily OFF time in Parkinson’s disease. Movement Disorders 28 (8), 1138–1141. https://doi.org/10.1002/mds.25418.

Namkoong, J., et al., 2007. Metabotropic glutamate receptor 1 and glutamate signaling in human melanoma. Cancer Res. 67 (5), 2298–2305. https://doi.org/10.1158/0008-5472.CAN-06-3665.

Ostrom, Q.T., et al., 2019. CBTRUS statistical report: primary brain and other central nervous system tumors diagnosed in the United States in 2012–2016. Neuro Oncol. 21 (Suppl. ment_5), v1–v100. https://doi.org/10.1093/neuonc/noz150.

Pettersen, E.F., et al., 2004. UCSF chimera—A visualization system for exploratory research and analysis. J. Comput. Chem. 25 (13), 1605–1612. https://doi.org/10.1002/jcc.20084.

Popoli, P., et al., 2002. Blockade of striatal adenosine A2A receptor reduces, through a presynaptic mechanism, quinolinic acid-induced excitotoxicity: possible relevance to neuroprotective interventions in neurodegenerative diseases of the striatum. J. Neurosci. 22 (5), 1967–1975. https://doi.org/10.1523/JNEUROSCI.22-05-01967.2002.

Price, D.J., Brooks III, C.L., 2004. A modified TIP3P water potential for simulation with ewald summation. J. Chem. Phys. 121 (20), 10096–10103. https://doi.org/10.1063/1.1808117.

Rosenblum, L.T., Trotti, D., 2017. EAAT2 and the molecular signature of amyotrophic lateral sclerosis. Adv. Neurobiol. 16, 117–136. https://doi.org/10.1007/978-3-319-55769-4_6.

Saitoh, Y., Takahashi, Y., 2020. Riluzole for the treatment of amyotrophic lateral sclerosis. Neurodegener. Dis. Manag. 10 (6), 343–355. https://doi.org/10.2217/nmt-2020-0033.

Sasaki, T., Kuniyasu, H., 2014. ‘significance of AKT in gastric cancer. Int. J. Oncol. 45 (6), 2187–2192. https://doi.org/10.3892/ijo.2014.2678 submitted for publication.

Spencer, K., et al., 2023. A phase I trial of riluzole and sorafenib in patients with advanced solid tumors: CTEP# 8850. Oncotarget 14, 302.doi. https://doi.org/10.18632/oncotarget.28403.

Sperling, S., et al., 2017. Riluzole: a potential therapeutic intervention in human brain tumor stem-like cells. Oncotarget 8 (57), 96697–96709. https://doi.org/10.18632/oncotarget.18043.

Speyer, C.L., et al., 2012. Metabotropic glutamate receptor-1: a potential therapeutic target for the treatment of breast cancer. Breast Cancer Res. Treat. 132 (2), 565–573. https://doi.org/10.1007/s10549-011-1624-x.

Speyer, C.L., et al., 2017. Riluzole synergizes with paclitaxel to inhibit cell growth and induce apoptosis in triple-negative breast cancer. Breast Cancer Res. Treat. 166 (2), 407–419. https://doi.org/10.1007/s10549-017-4435-x.

Stupp, R., et al., 2015. Maintenance therapy with tumor-treating fields plus temozolomide vs temozolomide alone for glioblastoma: a randomized clinical trial. JAMA 314 (23), 2535–2543. https://doi.org/10.1001/jama.2015.16669.

Stupp, R., et al., 2017. Effect of tumor-treating fields plus maintenance temozolomide vs maintenance temozolomide alone on survival in patients with glioblastoma: a randomized clinical trial. JAMA 318 (23), 2306–2316. https://doi.org/10.1001/jama.2017.18718.

Sun, L., et al., 2020. Riluzole enhances the response of human nasopharyngeal carcinoma cells to ionizing radiation via ATM/P53 signalling pathway. J. Cancer 11 (11), 3089–3098. https://doi.org/10.7150/jca.41217.

Sun, R., et al., 2021. The new role of riluzole in the treatment of pancreatic cancer through the apoptosis and autophagy pathways. J. Cell. Biochem. 122 (9), 934–944. https://doi.org/10.1002/jcb.29533.

Smith, M.A., Houghton, P., 2013. A Proposal Regarding Reporting of In Vitro Testing Results. Clinical Cancer Research 19 (11), 2828–2833. https://doi.org/10.1158/1078-0432.CCR-13-0043.

Tonazzini, I., et al., 2010. Multiscale morphology of organic semiconductor thin films controls the adhesion and viability of human neural cells. Biophys. J. 98 (12), 2804–2812. https://doi.org/10.1016/j.bpj.2010.03.036.

Trott, O., Olson, A.J., 2010. AutoDock vina: improving the speed and accuracy of docking with a new scoring function, efficient optimization, and multithreading. J. Comput. Chem. 31 (2), 455–461. https://doi.org/10.1002/jcc.21334.

Van Der Spoel, D., et al., 2005. GROMACS: fast, flexible, and free. J. Comput. Chem. 26 (16), 1701–1718. https://doi.org/10.1002/jcc.20291.

Vredenburgh, J.J., et al., 2007. Bevacizumab plus irinotecan in recurrent glioblastoma multiforme. J. Clin. Oncol. 25 (30), 4722–4729. https://doi.org/10.1200/JCO.2007.12.2440.

Wadosky, K.M., et al., 2019. Riluzole induces AR degradation via endoplasmic reticulum stress pathway in androgen-dependent and castration-resistant prostate cancer cells. Prostate 79 (2), 140–150. https://doi.org/10.1002/pros.23719.

Wang, Y., et al., 2021. Design, synthesis, and biological activity studies of istradefylline derivatives based on adenine as A2A receptor antagonists. ACS Omega 6 (6), 4386–4394. https://doi.org/10.1021/acsomega.0c05741.

Weller, M., et al., 1998. Predicting chemoresistance in human malignant glioma cells: the role of molecular genetic analyses. Int. J. Cancer 79 (6), 640–644. https://doi.org/10.1002/(SICI)1097-0215(19981218)79:6<640::AID-IJC15>3.0.CO;2-Z.

William, D., et al., 2018. Temozolomide-induced increase of tumorigenicity can be diminished by targeting of mitochondria in in vitro models of patient individual glioblastoma. PLoS One 13 (1), e0191511. https://doi.org/10.1371/journal.pone.0191511.

Wu, W., et al., 2021. Glioblastoma multiforme (GBM): an overview of current therapies and mechanisms of resistance. Pharmacol. Res. 171, 105780. https://doi.org/10.1016/j.phrs.2021.105780.

Xu, W., Baribault, H., Adamson, E.D., 1998. Vinculin knockout results in heart and brain defects during embryonic development. Development 125 (2), 327–337.

Yamada, T., et al., 2020. Riluzole enhances the antitumor effects of temozolomide via suppression of MGMT expression in glioblastoma. Journal of neurosurgery 134 (3), 701–710. https://doi.org/10.3171/2019.12.JNS192682.

Yip, D., et al., 2009. A phase 0 trial of riluzole in patients with resectable stage III and IV melanoma. Clin. Cancer Res. 15 (11), 3896–3902. https://doi.org/10.1158/1078-0432.CCR-08-3303.